# Enhancing Maneuverability via Gait Design

Siming Deng[1], Ross L. Hatton[2], and Noah J. Cowan[1]

***Abstract*— The gaits of locomoting systems are typically designed to maximize some sort of efficiency, such as cost of transport or speed. Equally important is the ability to modulate such a gait to effect turning maneuvers. For drag-dominated systems, geometric mechanics provides an elegant and practical framework for both ends—gait design and gait modulation. Within this framework, "constraint curvature" maps can be used to approximate the net displacement of robotic systems over cyclic gaits. Gait optimization is made possible under a previously reported "soap-bubble" algorithm. In this work, we propose both local and global gait morphing algorithms to modify a nominal gait to provide single-parameter steering control. Using a simplified swimmer, we numerically compare the two approaches and show that for modest turns, the local approach, while suboptimal, nevertheless proves effective for steering control. A potential advantage of the local approach is that it can be readily applied to soft robots or other systems where local approximations to the constraint curvature can be garnered from data, but for which obtaining an exact global model is infeasible.**

## I. INTRODUCTION

Often, the focus in locomotion research is on design of a nominal gait—for example, to minimize energy or maximize speed. However, maneuvering and steering are essential aspects in controlling a system. Though switching between a "forward" gait and a "turning" gait would provide a simple solution, continuous steering is crucial to allow a graceful means to respond to sensory feedback, avoid obstacles, or track moving targets. The value of such a graded steering control parameter becomes obvious when one considers driving a car, which would be awkward (at best) if the car only produced a finite set of discrete turning radii from which a driver (or algorithm) must select at each moment in time. By contrast, it would clearly be desirable to be able to exert continuous control over the steering direction. However, most complex undulatory robots—such as snake robots [1], [2] and legged systems [3], have no such built-in "steering wheel."

The problem we address in this paper is how to efficiently modulate an optimized forward gait to produce graded steering control, and effectively nudging the forward gait into a turning gait in a smooth fashion, analogous to a steering wheel in a car. Indeed, cockroaches exhibit graceful steering, as they modulate their gait to "servo" along walls, using tactile feedback from their antennae [4]. Inspired by cockroaches, engineering experts have devised smooth, but *ad hoc* steering control inputs for hexapods such as RHex [3] and Sprawl [5], by effectively inducing graded left–right asymmetries in the gait. The goal of this work is develop a principled way of constructing and exploiting such asymmetries for control.

The present work builds on a massive literature on maneuverability, but we focus narrowly on a few prior works most related to the present paper. Early work [2], [6] addressed how a multi-link snake-like robot that performs undulatory locomotion can make turns by offsetting its body curvature (i.e., steering can be achieved by regularizing the offset level), inducing a lateral asymmetry, a general idea later formalized in a seminal paper on steering control for cyclic, nonholonomic systems [7]. More recent work [8], [9] provided an approach to create gait libraries using a geometric mechanics framework, establishing the framework for maneuverability we build on in this paper.

Here, we aim to incorporate a previously published geometric optimization algorithm [10] to create general principled means by which to create effective, efficient modulations of a nominal gait for undulatory, drag-dominated robotic systems. If the locomotion model is a local, data-driven model [11]—only available in a neighborhood of the nominal gait—we present a computationally simple, local-gradient-based approach. But if the locomotor model is global (e.g., built from first principles), we can apply an (approximately) globally optimal approach. Then we compare the performance between the approaches through numerical simulations in a simplified swimmer.

## II. BACKGROUND

In this paper will use Purcell's three link swimmer [12] as an example system to test our gait modulation methods (Fig. 1). The three link model is widely adopted because its simple dynamics can be easily visualized on a two-dimensional shape space.

### A. Locomotion Model

When analyzing a system's locomotor behavior, it is convenient to separate its configuration space $Q$ into its shape space $M$ and position space $G$, namely $Q = G \times M$. A system's shape (i.e., its joint configuration) $r \in M$ defines its internal configuration—namely, where each body segment

*This material is based upon work supported by the National Science Foundation under grants no. #1830893, EFRI C3 SoRo: Programming Thermobiochemomechanical (TBCM) Multiplex Robot Gels, #1935324 EFRI C3 SoRo: Control of Local Curvature and Buckling for Multifunctional Textile-Based Robots, and #1653220 CAREER: Geometric Understanding of Locomotion

[1]S. Deng and N. J. Cowan are with the Laboratory for Computational Sensing and Robotics, and the Department of Mechanical Engineering, Johns Hopkins University, Baltimore MD 21218 USA. <sdeng10, ncowan>@jhu.edu

[2]R. L. Hatton is with the Collaborative Robotics and Intelligent Systems (CoRIS) Institute, and the Department of Mechanical, Industrial & Manufacturing Engineering, Oregon State University, Corvallis, OR 97331 USA. Ross.Hatton@oregonstate.edu

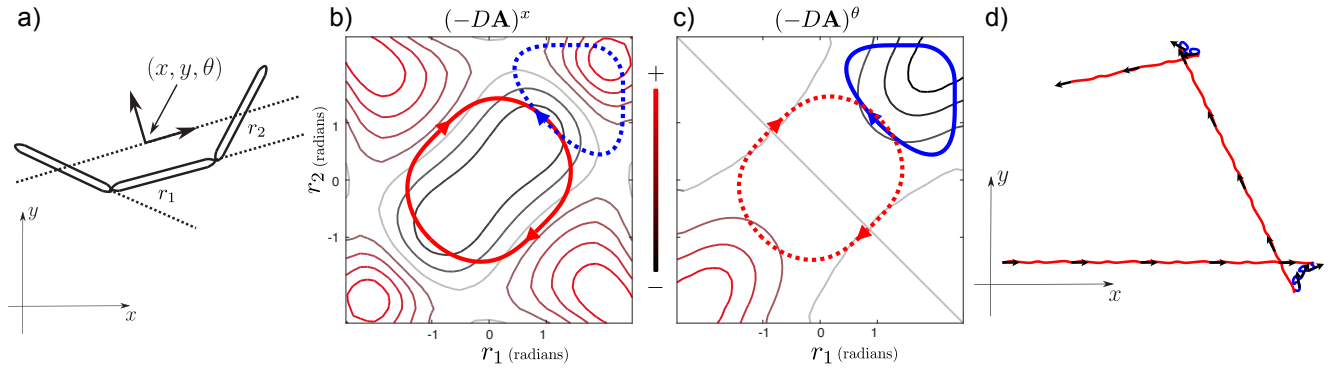


Fig. 1. An overview of an example system and its optimal gaits. (a) Schematic of a three-link viscous swimmer—a minimal template [13] for understanding locomotion. The shape of the system, described by its two joint positions, lives in a two-dimensional space. The coordinate of the body frame is chosen according to the *minimal perturbation* principle [14]. (b) The optimal gait (red) in the sense of $x$-direction motion efficiency (i.e. the largest displacement in x-direction per unit power dissipation). The gait is plotted over the system's *constraint curvature* height function corresponding to x-direction movement $(-D\boldsymbol{A})^x$, which provides an approximation to the system's locomotor behavior. (c) Similar to (b), the optimal gait (blue) for turning motion. The two optimal gaits are cross-illustrated in both (b) and (c) with dashed curves. (d) A trivial demonstration of the system's spatial trajectory from a gait-switching execution. The black arrows over the trajectory denotes the system's x-axis at the beginning of each cycle, and the color coded trajectory represents which gait the system is operating on.

is located with respect to a body-fixed frame. Meanwhile, its global position $g \in G$ ( $\mathrm{SE}(2)$ for a planar system) locates the system in a spatial frame, specifying the location and orientation of the body frame. The three link swimmer is considered a planar system with a two-DoF shape space, namely $g \in \mathrm{SE}(2)$ and $r = [r_1, r_2]^T$. In the sequel, when convenient, we will conflate $g$ with its (global) coordinate representation, namely $g = [g_x, g_y, g_\theta]^T$.

For a drag-dominated system (i.e., a system with negligible inertial effects), the body velocity is related to its shape velocities by the local connection [15], [16]:

$$g^{-1}\dot{g} = -\boldsymbol{A}(r)\dot{r}, \tag{1}$$

where $g^{-1}\dot{g}$ is the body frame velocity of the system, $r \in M$ denotes the system's internal shape variable, and $\boldsymbol{A(r)}$ is the local connection matrix. The local connection matrix $\boldsymbol{A(r)}$ contains all the information of the system's locomotor behavior in the environment; it acts analogously to a Jacobian in that it maps velocities in one coordinate to velocities in another (however, unlike a Jacobian matrix, it is generally non-integrable). The net spacial displacement of performing one gait can be calculated with a path integral over the local connection vector fields:

$$g_\phi = \begin{bmatrix} g_x \\ g_y \\ g_\theta \end{bmatrix} = \oint_\phi -g\boldsymbol{A}(r) \tag{2}$$

where $g_\phi$ denote the net displacement generated executing one cycle of gait $\phi$. Previous works [17] show that we can simplify this line integral by a surface integral as follows:

$$g_\phi \approx \exp\left(\iint_{\phi_a} (-D\boldsymbol{A})\right) \tag{3}$$

where $(-D\boldsymbol{A}) = \boldsymbol{dA} + \sum_{i<j}[A_i, A_j]$ is the total Lie bracket of the local connection. Here, $\boldsymbol{dA}$ is the exterior derivative, and $\sum_{i<j}[A_i, A_j]$ is the sum of Lie brackets between the columns of $\boldsymbol{A}$.

Another important aspect to a drag-dominated system is the effort required when changing shape, which can be modeled as the path-length $s$ of the system shape trajectory weighted by a Riemannian metric $\mathcal{M}$

$$ds^2 = dr^T \mathcal{M} dr, \tag{4}$$

that encodes the actual effort required to move the links through the surrounding fluid [18], [19], [12].

### B. Gait Optimization

Given a gait parametrization $p$, optimal cycles must satisfy the following gradient condition [10]

$$\nabla_p J = \mathbf{0} \tag{5}$$

where $J$ is an objective functional. For example, we consider

$$J_x = \frac{g_x}{s} \tag{6}$$

as the objective functional that captures how efficient the gait is in terms of moving forward, regularized by its path-length. Similar objective functionals can be defined in terms of rotation or lateral motion. Solutions to (5) for the cost (6) can be reached by finding the equilibria of the dynamical system

$$\dot{p} = \nabla_p J_x = \frac{1}{s}\nabla_p g_x - \frac{g_x}{s^2}\nabla_p s + \nabla_p \sigma, \tag{7}$$

where $g$, $s$ denote the spatial displacement and the path-length cost, executing one cycle of the gait $\phi$. The other terms in the expression will be described below.

The first term $\nabla_p g_x$ alone would lead to a gait that has the greatest displacement per cycle, corresponding to the simple objective $g_x$. The approximation in (3) is a surface integral whose boundary is defined by the gait $\phi$; hence a variation around gait $\phi$ is intuitively thought of as adding

or subtracting weighted regions near the surface boundary. Formally, the general form of the *Leibniz rule*[1] converts this gradient of the functional with respect to variations of its boundary to the gradient of its boundary weighted by the integrand:

$$\nabla_p \iint_{\phi_a} (-D\boldsymbol{A})^x = \oint_{\phi} (\nabla_p \phi) \lrcorner (-D\boldsymbol{A})^x. \tag{8}$$

Specifically, the sign $\lrcorner$ denotes the *interior product*[2] between the boundary gradient $\nabla_p \phi$ and the weight $(-D\boldsymbol{A})^x$. In the simple setting that we consider here, a system with a two-dimensional shape space, the above interior product reduces to a normal multiplication between the normal component of $\nabla_p \phi$ and the scalar magnitude of the constraint curvature,

$$\nabla_p \iint_{\phi_a} (-D\boldsymbol{A})^x = \oint_{\phi} (\nabla_{p\perp} \phi)(-D\boldsymbol{A})^x. \tag{9}$$

Running the optimization with only the first term will end up with gaits locating on the zero contour of the constraint curvature.

The second term $\nabla_p s$ in (7) measures how variations of gait affect its execution cost per cycle. This term acts to regularize the optimization, cutting off diminishing returns around low-yield regions on the constraint curvature map. The third term $\nabla_p \sigma$ in (7) is responsible for reorganizing waypoints in the local tangent direction to achieve the most efficient pacing when executing the gait. This term applies changes that keep the gait within the same image-family.[3] For the dissipative mechanical systems that we consider here, this gradient term is orthogonal to the other two terms mentioned above; this implies that the optimization of efficient pacing is independent from the path optimization.

For the example system that we consider for this paper, the optimal gaits, that are generated by previously discussed algorithm, maximizing $x$ and $\theta$ motion efficiencies are shown in Fig. 1, respectively. The optimal gaits each encircle a rich, sign-definite region, where it gives up the low-yield regions for shorter path-length, on their respective constraint curvature maps.

## III. Maneuverability

A common scenario in locomotion is steering during forward motion–e.g., a robot executing a translational gait, and modulating this nominal gait to accomplish graded rotational redirection of the heading. Ideally, such steering occurs while largely preserving the overall translational motion. In essence, we are looking for a smooth transformation from the optimum under one objective (e.g. pure forward motion) to the optimum under another objective (e.g. pure rotational motion). Depending on how much information we know about the model, we can generate such transformation of gaits with local or global approaches. In the following subsections, we discuss the local and global methods respectively under the setting of enhancing turning around a forward-moving gait.

### A. Gradient-Based Approaches

The gradients of displacement and cost with respect to the gait parameters provide locally optimal changes with respect to the new objective. Tweaking the gait along the gradient direction will produce the fastest changes in the outcome; in other words, the modulated gait will have significant changes under the new objective with minimal modulation.

Under the previously mentioned setting, to modulate around an optimal forward gait in order to achieve turning, we initiate at the optimal gait in the sense of the most efficient $x$ displacement as mentioned in II-B:

$$p_x : \nabla_p J_x = \nabla_p \frac{g_x}{s} = \mathbf{0}. \tag{10}$$

Modulating this starting gait along the gradient $\nabla_p J_\theta$ will provide the most rapid changes of $J_\theta$, rotational efficiency. Then, the solution of the following equation will guide the gait toward the rotational optimum:

$$\frac{dp}{du} = \nabla_p J_\theta, \quad p(0) = p_x, \tag{11}$$

where $p_x$ denote the optimal forward gait parameters. The solution $p(u)$ can be pre-calculated and stored as an infinite-dimensional gait library where $u$ serves as the modulation variable.

Calculating the above solution will require the model information (i.e. the constraint curvature) at each iteration during the process; visually it is the shape space area swept by the gait library. In situations where we do not have the luxury of knowing the full model, as mentioned in Section I, it is viable to simply use the first order approximation as the following:

$$p(u) = p_x + u \nabla_p J_\theta|_{p_x}, \tag{12}$$

where $\nabla_p J_\theta|_{p_x}$ is the first gradient at the x-direction optimum. As a comparison, the first order approximation requires less model information as well as less computational power while maintaining similar performance within some range of turning behavior (see Results, Section IV).

### B. Pareto Front

Now assume we have the full locomotion model, and we would like to push for the optimal transition from one optimum to another. Here we consider the trade-off between $x$ and $\theta$ efficiencies in the sense of Pareto optimality, where we cannot improve one objective without hurting the other. A set of Pareto optimal gaits can be generated, forming a Pareto front, using the following objective in our optimization algorithm while iterating $\alpha$ from 0 to 1:

$$J_{total} = \alpha \frac{J_x}{J_{xmax}} + (1-\alpha) \frac{J_\theta}{J_{\theta max}}, \tag{13}$$

where $J_x$ and $J_\theta$ are normalized using the optimal values in each direction alone $J_{xmax}$ $J_{\theta max}$.

[1] See [20] for more details

[2] An operation between a vector field and a differential form that results in a -1 degree differential form by "pre-specifying" the vector field as one of the inputs to the differential form. See more in [20].

[3] The image-family of a gait is the set of all gaits that share the same image in the shape space

Although the above method can guarantee global optimality to the objective $J_{total}$ without being trapped at local optima (i.e., critical points) like the gradient-based methods, it cannot guarantee a smooth transition among gaits located on the Pareto Front. We will continue the comparison between this global method and previous gradient-based methods in Results (Section IV).

### C. Online Control

In general it takes a handful of parameters to describe gaits, and the outcome of gaits are of relatively small size (i.e., SE(2) has only 3 degree of freedom). A higher level control is useful in simplifying the control complexity. Previously discussed gait modulation naturally enables a high level control over the robot movement despite its complex locomotor behavior.

In an online, within-cycle type of control scenario, gait switching/modulation can happen at phases where gaits are not collocated. Large-amplitude "jumps" can cause the robot to stop current motion, reposition its joints, then finally follow the new gait, which in general can badly affect the overall smoothness and efficiency of the system motion. Limiting the band-width of modulation rate can prevent jumps from one gait to another. This limitation acts intuitively like a dynamically adjusted interpolation between current and target gaits.

In an online control situation, the commanded shape velocity $\dot{r}$ is constructed as

$$\dot{r}(t) = \dot{r}^* + \dot{u}d(t) + u\dot{d}(t), \tag{14}$$

where $\dot{r}^*$ denotes the shape velocity along the current gait, $u$ denotes the control variable providing steer-ability, and $d(t)$ denotes the difference between current gait and target gait at time $t$. Because drag-dominated systems are most efficient when their power dissipation is held constant, we want to limit $\dot{u}$ such that it does not significantly impact the metric-weighted speed of the system,

$$\|\dot{r}\|_{\mathcal{M}} \approx \|\dot{r}^* + u\dot{d}(t)\|_{\mathcal{M}}. \tag{15}$$

In the demonstration below, we implement this restriction enforcing

$$\|\dot{u}d(t)\|_{\mathcal{M}} \leq k\|\dot{r}\|_{\mathcal{M}}, \quad 0 < k \ll 1. \tag{16}$$

## IV. Results

In this section we provide a parallel comparison among different approaches in generating gait modulations using the example simulated system three-link swimmer mentioned in II. Also the following results are generated under the circumstance where an optimal forward gait is modulated for turning.

Following the methods mentioned in III-A, a number of snapshots from the solution of (11), $p(u)$, are shown in Fig. 2(a). As expected, as the modulation variable $u$ increases, the gradient pulls the gaits toward the top-right corner, where the optimal rotation gait is located (see Fig. 1(b)).

As discussed in III-A, under waypoint parametrization, the gradient is given by local definitions along the gait.

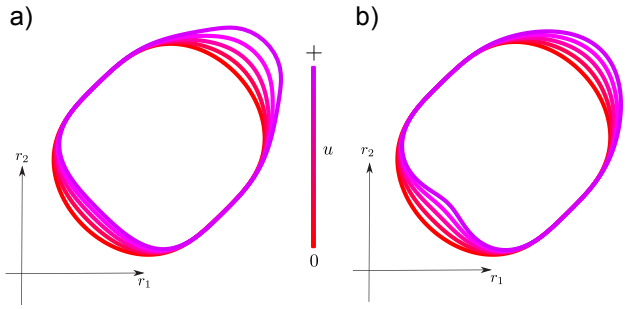


Fig. 2. An illustration of gait modulations generated with (a) gradient iteration and (b) first order approximation at the nominal gait. When the modulation variable $u = 0$, the gait (red) is the x-direction optimal gait (i.e., the same as the one shown in Fig. 1(b)). As $u$ increase in value, the nominal gait is modulated toward the top-right corner for additional $\theta$ movement.

Consequently, part of the gait can be trapped in some local critical points, where the gradient diminishes for some waypoints, even though other parts of the gait are advancing with the gradient. In Fig. 2(a), the gradient along the two sides (top-left and bottom-right) started as zeros, leaving no changes across modulations. Similarly, as the bottom-left side of the gait gets close to a local critical point, this side converges and is not able to proceed onward.

The first order approximation results the gait modulation in a linear fashion as expected. The effect on the bottom-left side differs from the one mentioned above; because the gradient is non-zero at start, that side will keep modulating even though it causes additional unnecessary path-length costs by dimpling inwards.

There is a significant gap in the middle of the Pareto Front (see Fig. 3) around $\alpha = 0.4$, where the optimizer is giving up a large amount of x-direction efficiency in return of $\theta$-direction efficiency. We conjecture that the formation of such a bifurcation region is due to the balancing of two local optima in $x$ and $\theta$ efficiencies, similar to those observed in the gradient iteration method. Around the region near $\alpha = 0.4$, the two local optima yield close values. As $J_{total}$ is altered by $\alpha$, the global optimum has a sudden jump, both in the appearance of the gait and the motion output. Further investigation is needed to make a conclusion here.

Intuitively such bifurcation is reasonable, where there are certain limits to the extents that modulating a gait is meaningful, once beyond that limit, then it is time to switch to some other qualitatively different gait.

Fig. 4(a) shows a zoomed-in view of the three methods on the trade-off map between $x$ and $\theta$ efficiencies, focusing at the region close the x-direction optimum (bottom right corner of Fig. 3). The efficiency of gradient-based methods slowly drop off as they move towards turning, part of the reason being segments of the gait are trapped at local critical points.

## V. Demonstration

We implemented our gait modulation generation along with an additional command filter control described in III-C.

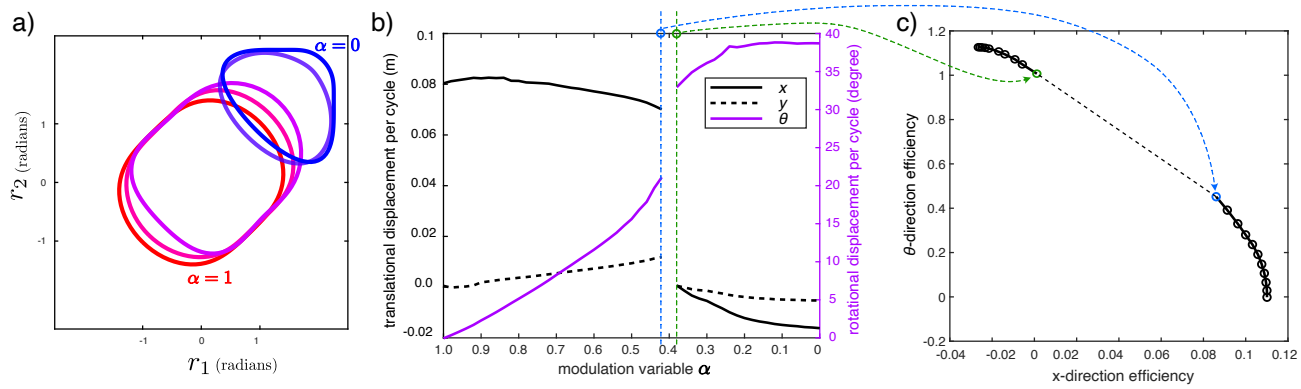


Fig. 3. An overview of the performance of the gait libraries from the global approach. (a) Gaits generated with the global approach, where $\alpha = 1, 0$ corresponds to those optimal gaits shown in Fig. 1(b-c). (b) Displacement in $(x, y, \theta)$ per cycle of the gait library. Note that the discontinuity appears around the region $\alpha = 0.4$ where the optimizer decides to qualitatively change the gait. (c) Pareto front, generated from (13), on the efficiency trade-off map. The discontinuity appears here as a large gap where the optimizer was not able to reliably converge to data points in between, likely due to a bifurcation in the objective function as a function of $\alpha$.

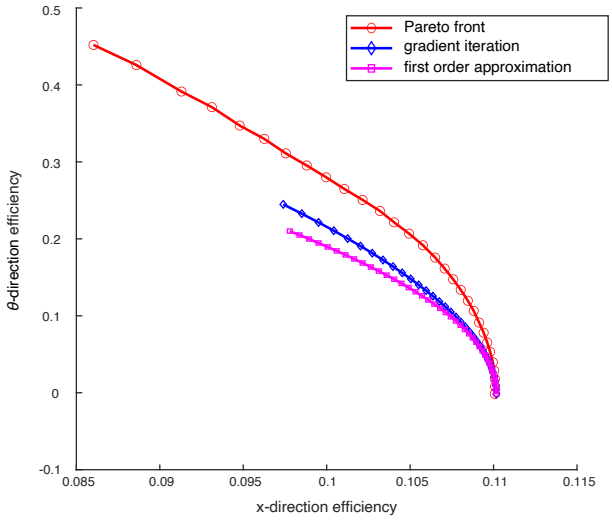


Fig. 4. An efficiency comparison between the gait modulations generated by local and global approaches. The performance of the gradient-based methods is almost as good as the global optimizer locally at the x-optimum, and slowly drops off.

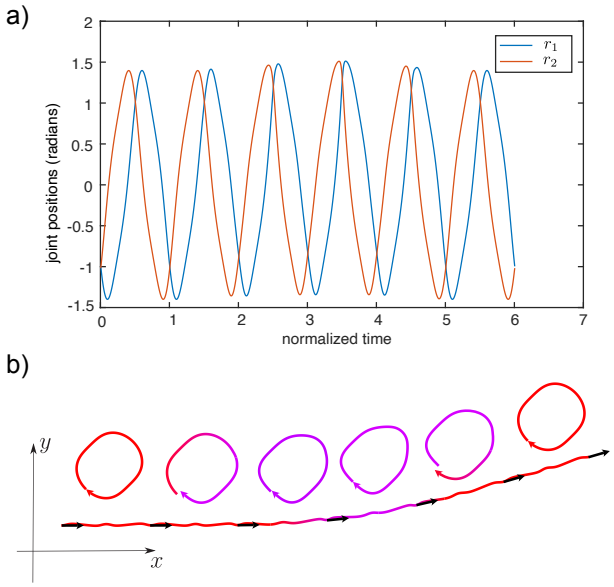


Fig. 5. A demonstration of gait modulation in motion. (a) Shape trajectory, as quasi-periodic functions, of the robot over a normalized time (i.e. one full lap in the shape space per normalized time). (b) The system's spatial trajectory by executing the above shapes. Black arrows denotes the system's x-axis position at the beginning of each lap, and the color coded trajectory shows approximately (not to scale) the average turning curvature is currently being performed. The shape space trajectory of each lap is also shown above the trajectory as a simple visualization.

The following demonstration is made on the same example system as in previous sections, the gait libraries are generated by the gradient iteration methods.

We chose turning curvature as as an intuitive control input. For the gait modulations, average turning curvature, which is a function of the $x$ and $\theta$ displacements induced by executing one full gait cycle, was used to map desired curvature to the gait modulation variable $u$. Under an arbitrary command (i.e., to perform a slight turn during forward motion), the controller limits the rate of modulation variable, $\dot{u}$, based on the differences between current and target shape as discussed in (16), where $k$ is set to 0.1. The gait trajectory in Fig. 5 is as expected, when at a phase where current gait and target gait are not collocated, the command filter will dynamically interpolate between the two gaits, preventing sudden jumps in the shape space.

## VI. Discussion

In this paper, we incorporate insights from geometric gait optimization to construct gait modulations that enable "controllable maneuverability". The local approach we present involves starting with a forward-optimized gait, and then inducing gait parameter modulations that push the gait in the gradient direction of a turning objective function; this local strategy provides an effective turning control system up to

moderate turns, according to our numerical investigation of a simplified swimmer. The global approach aims to generate a continuous family of optimal gaits that satisfy Pareto optimality—trading of forward movement and turning. We also discussed the advantages and limitations between local and global approaches in generating gait modulations.

Finally, we demonstrated a common use case of gait modulations, where a high-level continuous steering control is possible while largely maintaining a nominal forward gait.

More broadly, one of our future aims is to apply principles from this geometric framework to make steerable, stimuli-based soft robots. Our groups work with experts in material science and mechanics who focus on fabrication and modeling of stimulus-responsive materials [21], [22] and of nonlinear high-deformation structures [23].

Some early works [24] are successful in building hydrogel-based origami structures in which they are able to achieve a variety of shape changes including bending, elongating, twisting, and buckling. From a roboticist point of view, these shape changes can be utilized as actuation for soft robots. On the other hand, there is no obvious way to build low-dimensional, first-principles models for the locomotor dynamics—making our interest in using local maneuvering based on data-driven models [11] particularly salient. Ultimately, we are interested in putting together micro-scaled, hydrogel-based soft robots that locomote and perform a wide range of dynamic, maneuverable locomotor tasks based on environmental information.

For the high-deformation structures, a key focus of future work will be understanding how to access the steering modulations when only some of the shape variables are directly controlled. This work will combine the ideas outlined in this paper with the geometric mechanics of semi-passive locomotion we explored in [25].

## REFERENCES


[1] C. Ye, S. Ma, B. Li, and Y. Wang, "Turning and side motion of snake-like robot," in *IEEE International Conference on Robotics and Automation, 2004. Proceedings. ICRA '04. 2004*, vol. 5, 2004, pp. 5075–5080.

[2] S. Hirose, "Biologically inspired robots: Snake-like locomotors and manipulators," 1993.

[3] U. Saranli, M. Buehler, and D. E. Koditschek, "RHex: A simple and highly mobile hexapod robot," *The International Journal of Robotics Research*, vol. 20, no. 7, pp. 616–631, 2001.

[4] J. Lee, S. N. Sponberg, O. Y. Loh, A. G. Lamperski, R. J. Full, and N. J. Cowan, "Templates and anchors for antenna-based wall following in cockroaches and robots," *IEEE Trans Robot*, vol. 24, no. 1, pp. 130–143, 2008.

[5] N. J. Cowan, E. J. Ma, M. Cutkosky, and R. J. Full, "A biologically inspired passive antenna for steering control of a running robot," in *Robotics Research*, ser. Springer Tracts in Advanced Robotics. Siena, Italy: Springer, 2003, pp. 540–550.

[6] M. Sfakiotakis and D. Tsakiris, "Biomimetic centering for undulatory robots," *International Journal of Robotics Research*, November/December 2007.

[7] R. Murray and S. S. Sastry, "Nonholonomic motion planning: Steering using sinusoids," EECS Department, University of California, Berkeley, Tech. Rep. UCB/ERL M91/45, May 1991.

[8] B. Bittner and S. Revzen, "Optimizing gait libraries via a coverage metric," *arXiv:2107.08775*, 2021.

[9] R. L. Hatton, L. J. Burton, A. E. Hosoi, and H. Choset, "Geometric maneuverability with applications to low reynolds number swimming," in *2011 IEEE/RSJ International Conference on Intelligent Robots and Systems*, 2011, pp. 3893–3898.

[10] S. Ramasamy and R. L. Hatton, "The geometry of optimal gaits for drag-dominated kinematic systems," *IEEE Transactions on Robotics*, vol. 35, no. 4, pp. 1014–1033, 2019.

[11] B. Bittner, R. L. Hatton, and S. Revzen, "Geometrically optimal gaits: a data-driven approach," *Nonlinear Dynamics*, vol. 94, no. 3, pp. 1933–1948, 2018.

[12] L. Becker and H. Stone, "On self-propulsion of micro-machines at low reynolds number: Purcell's three-link swimmer," *Journal of Fluid Mechanics*, vol. 490, pp. 15 – 35, 09 2003.

[13] R. J. Full and D. E. Koditschek, "Templates and anchors: neuromechanical hypotheses of legged locomotion on land," *Journal of Experimental Biology*, vol. 202, no. 23, pp. 3325–3332, dec 1999.

[14] R. L. Hatton and H. Choset, "Geometric motion planning: The local connection, stokes' theorem, and the importance of coordinate choice," *The International Journal of Robotics Research*, vol. 30, no. 8, pp. 988–1014, 2011.

[15] S. D. Kelly and R. M. Murray, "Geometric phases and robotic locomotion," *Journal of Robotic Systems*, vol. 12, no. 6, pp. 417–431, 1995.

[16] R. Hatton and H. Choset, "Approximating displacement with the body velocity integral," June 2009.

[17] R. L. Hatton and H. Choset, "Nonconservativity and noncommutativity in locomotion," *The European Physical Journal Special Topics*, vol. 224, no. 17, pp. 3141–3174, 2015.

[18] ——, *Kinematic Cartography for Locomotion at Low Reynolds Numbers*, 2012, pp. 113–120.

[19] R. L. Hatton, T. Dear, and H. Choset, "Kinematic cartography and the efficiency of viscous swimming," *IEEE Transactions on Robotics*, vol. 33, no. 3, pp. 523–535, 2017.

[20] H. Flanders, "Differentiation under the integral sign," *American Mathematical Monthly*, vol. 80, pp. 615–627, 1973.

[21] R. Shi, J. Fern, W. Xu, S. Jia, Q. Huang, G. Pahapale, R. Schulman, and D. H. Gracias, "Multicomponent dna polymerization motor gels," *Small*, vol. 16, no. 37, p. 2002946, 2020.

[22] A. Cangialosi, C. Yoon, J. Liu, Q. Huang, J. Guo, T. D. Nguyen, D. H. Gracias, and R. Schulman, "Dna sequence–directed shape change of photopatterned hydrogels via high-degree swelling," *Science*, vol. 357, no. 6356, pp. 1126–1130, 2017.

[23] M. Sharifzadeh, Y. Jiang, and D. M. Aukes, "Reconfigurable curved beams for selectable swimming gaits in an underwater robot," *IEEE Robotics and Automation Letters*, vol. 6, no. 2, pp. 3437–3444, 2021.

[24] J. Liu, O. Erol, A. Pantula, W. Liu, Z. Jiang, K. Kobayashi, D. Chatterjee, N. Hibino, L. H. Romer, S. H. Kang, T. D. Nguyen, and D. H. Gracias, "Dual-gel 4d printing of bioinspired tubes," *ACS Applied Materials & Interfaces*, vol. 11, no. 8, pp. 8492–8498, feb 2019.

[25] S. Ramasamy and R. L. Hatton, "Optimal gaits for drag-dominated swimmers with passive elastic joints," *Phys. Rev. E*, vol. 103, p. 032605, Mar 2021. [Online]. Available: https://link.aps.org/doi/10.1103/PhysRevE.103.032605